Human Molecular Genetics, 2011, Vol. 20, No. 13 **2535–2548**
doi:10.1093/hmg/ddr152
Advance Access published on April 14, 2011

Muscle pathology without severe nerve pathology in a new mouse model of Charcot–Marie–Tooth disease type 2E

Hailian Shen[1,†], Devin M. Barry[1,2], Jeffrey M. Dale[1,2], Virginia B. Garcia[2], Nigel A. Calcutt[3] and Michael L. Garcia[1,2,*]

[1]Department of Biological Sciences and [2]C.S. Bond Life Sciences Center, University of Missouri, Columbia, MO 65211, USA and [3]Department of Pathology, University of California San Diego, La Jolla, CA 92093, USA

Received January 13, 2011; Revised March 7, 2011; Accepted April 4, 2011

Mutations in neurofilament light (NF-L) have been linked to Charcot–Marie–Tooth disease type 2E (CMT2E) in humans. To provide insight into disease pathogenesis, we developed a novel line of CMT2E mice that constitutively express human NF-L (hNF-L) with a glutamic acid to lysine mutation at position 397 (hNF-L^{E397K}). This new line of mice developed signs consistent with CMT2E patients. Disease signs were first observed at 4 months in hNF-L^{E397K} mice, and consisted of aberrant hind limb posture, digit deformities, reduced voluntary locomotor activity, reduced motor nerve conduction velocities (MNCVs) and muscle atrophy. Reduced voluntary locomotor activity and muscle pathology occurred without significant denervation, and hNF-L^{E397K} mice showed relatively mild signs of nerve pathology. Nerve pathology in hNF-L^{E397K} mice was characterized by ectopic accumulations of phosphorylated NFs in motor neuron cell bodies as early as 1 month. Moreover, NF organization was altered in motor and sensory roots, with small motor axons being most affected. Peak axonal diameter was reduced for small motor axons prior to and after the onset of overt phenotypes, whereas large motor axons were affected only after onset, which correlated with reduced MNCVs. Additionally, there was a small reduction in the number of sensory axons in symptomatic hNF-L^{E397K} mice. hNF-L^{E397K} mice are a novel line of CMT2E mice that recapitulate many of the overt phenotypes observed in CMT2E patients and hNF-L^{P22S} mice. The cellular pathology observed in hNF-L^{E397K} mice differed from that recently reported in hNF-L^{P22S} mice, suggesting that overt CMT2E phenotypes may arise through different cellular mechanisms.

INTRODUCTION

Charcot–Marie–Tooth disease (CMT) is the most commonly inherited peripheral neuropathy (1,2). CMT neuropathies are grouped into four main types, CMT1-4, based on the specific genetic defect. Moreover, each type of CMT has several subtypes. CMT2E is a predominantly autosomal dominant subtype of CMT2. Until recently, the cause of CMT2E remained obscure. Genome-wide screening pinpointed the disease locus in a family of CMT2E patients to 8p21 within a 16 cM interval (3). Sequencing revealed the first CMT2E mutation in the neurofilament light gene (*nefl*). Subsequently, 14 additional missense, 2 deletion and 2 nonsense mutations in the NF-L gene have been linked to CMT2E (3–11).

Neurofilaments (NFs) are obligate heteropolymers of NF light (NF-L), medium (NF-M) and heavy (NF-H) proteins (12,13) within mature peripheral nerves. Within the central nervous system, α-internexin also co-assembles with NFs to form the classic 10 nm filament (14). NFs are intrinsic determinants of axonal volume within myelinated nerve segments. The mechanism by which NFs regulate axonal volume remains to be determined. However, loss of NF-L, by a spontaneous nonsense mutation in quail (15) or by targeted deletion

*To whom correspondence should be addressed at: University of Missouri, 340C C.S. Bond Life Sciences Center, 1201 Rollins Road, Columbia, MO 65211, USA. Tel: +1 5738829712; Fax: +1 5738849395; Email: garciaml@missouri.edu
†Present address: Department of Neurology, LRB 670Z, University of Massachusetts Medical School, 364 Plantation Street, Worcester, MA 01605, USA.

in mouse (16), resulted in axons with reduced diameters and slowed conduction velocities (17,18).

NF-L-linked CMT2E mutations are distributed throughout the functional domains of NF-L (Fig. 1A). Co-expression of most NF-L mutants with wild-type NF-M or NF-H subunits, in cell lines, disrupted the NF cytoskeleton, resulting in the formation of aggregates within the cell body (19–21). Moreover, expression of NF-L^{P8R} and NF-L^{Q333P} in primary neuronal cells acted in a dominant manner disrupting the endogenous NF network and reducing the transport of both NFs and mitochondria into axons (19). Recently, an animal model of CMT2E was developed expressing an inducible hNF-L^{P22S} transgene [human NF-L (hNF-L)] (22). The mouse developed signs that are associated with clinical CMT, such as aberrant hind limb posture and motor deficits (22). Analysis of hind limbs indicated that the muscles were hypertrophied with a significant reduction in the number of innervated fibers (22). Interestingly, suppressing expression of the hNF-L^{P22S} transgene, by providing doxycycline, rapidly reversed these phenotypes (22).

We report the generation of a novel line of CMT2E mice expressing hNF-L in which there was a glutamic acid to lysine mutation at amino acid 397 (Fig. 1A, boxed mutation). As with the hNF-L^{P22S} mice, this new line of mice developed phenotypes that are associated with CMT such as aberrant hind limb posture and digit deformities. However, there were important differences between the two lines of CMT2E mice. Consistent with the clinical presentation, muscles of hNF-L^{E397K} mice were atrophied. Additionally, significant denervation of hind limb muscles of hNF-L^{E397K} mice was not observed. The differences in cellular pathology between the two animal models may provide insights into the heterogeneity of CMT2E progression in humans.

RESULTS

Generation of hNF-L and hNF-L^{E397K} mice

Eighteen mutations in hNF-L have been linked to CMT2E (Fig. 1A). These mutations span all functional domains of the protein. We have focused on glutamic acid to lysine mutation at position 397, which is located in the most highly conserved sequence in the intermediate filament family (the KLLEGEE motif). We used site-directed mutagenesis to introduce a G-to-A nucleotide substitution at nucleotide 3332 of human *nefl* gene, resulting in a glutamic acid-to-lysine substitution in the resulting protein. Four lines of mice expressing either wild-type hNF-L or hNF-L^{E397K} were obtained. Genotyping was performed by PCR analysis of mouse genomic DNA obtained from tail biopsies (results for three of the four mouse lines are shown in Fig. 1B). The human-specific primers failed to amplify a product from non-transgenic control mice (lane 4 in the upper panel and lanes 3–5 in the lower panel of Fig. 1B). Expression of either wild-type or mutant hNF-L did not affect the transcription of other endogenous mouse NF genes or of a neuron-specific isoform of tubulin (βIII-tubulin) (Fig. 1C). Driving expression of wild-type and mutant hNF-L utilizing the endogenous hNF-L promoter resulted in low expression levels of hNF-L in both wild-type and hNF-L^{E397K} mice (Fig. 1D). Translation of hNF-L transgenes did not affect the translation or stability of endogenous mouse NFs or βIII-tubulin (Fig. 1D). Moreover, the human transgenes did not result in ectopic expression of hNF-L in young (Fig. 1E) or aged (Fig. 1F) mice.

Owing to the relatively low levels of hNF-L protein, we wanted to ensure that our antibodies were indeed recognizing hNF-L and not cross-reacting with the more abundant endogenous NF-L. Therefore, we bred mice expressing wild-type and mutant hNF-L with mice in which mouse NF-L has been deleted (NF-L$^{-/-}$) (Fig. 2A). In NF-L$^{-/-}$ mice, no NF-L was detectable. However, in NF-L$^{-/-}$;hNF-L and NF-L$^{-/-}$;hNF-L^{E397K} mice, hNF-L was detected, supporting our first results that hNF-L transgenes resulted in low levels of hNF-L expression (Fig. 2A). Relative optical densities were determined for each genotype (Fig. 2B), and proteins were normalized to GAPDH. hNF-L^{E397K} protein levels were below endogenous NF-L and hNF-L levels (Fig. 2B).

hNF-L^{E397K} mice develop aberrant hind limb posture and digit deformities

CMT is associated with aberrant lower limb posture and deformities of feet (23). To determine whether hNF-L^{E397K} mice displayed phenotypes associated with CMT, hNF-L and hNF-L^{E397K} mice were induced to spread their hind limbs and digits. When lifted by the tail, hNF-L mice spread both hind limbs and all digits of the hind limb paws (Fig. 3A). However, hNF-L^{E397K} mice were not able to spread their hind limbs (Fig. 3B–D). Moreover, the lower joints appeared stiff, and the digits of the hind limb curled instead of spreading. In some hNF-L^{E397K} mice, the phenotype in the hind limb digits appeared unilaterally, whereas other hNF-L^{E397K} mice initially displayed a unilateral phenotype progressing to a bilateral phenotype (Fig. 3B–D). Signs of hind limb weakness and digit abnormalities were observable as early as 4 months in hNF-L^{E397K} mice. Despite having signs associated with hind limb weakness, hNF-L^{E397K} mice did not show alterations in body mass, which is taken as an indication of overall muscle mass, relative to mice expressing wild-type hNF-L (Fig. 3E).

hNF-L and hNF-L^{E397K} mice were given free access to running wheels for 1 week. The distance run was recorded each day. hNF-L line 673 and hNF-L^{E397K} line 730 were originally monitored. hNF-L^{E397K} mice had reduced levels of locomotor activity relative to hNF-L controls every night (Fig. 4A). However, these differences did not reach statistical significance with the exception of nights 3–5. The total distance run over the course of a week was reduced in hNF-L^{E397K} mice (Fig. 4B). To determine whether reduced activity was limited to a single line of hNF-L^{E397K} mice, we monitored activity for all lines of mice. Again, hNF-L^{E397K} mice had reduced locomotor activity every night, with nights 1 and 3–5 reaching statistical significance (Fig. 4C). Total distance run was also significantly reduced in all lines of hNF-L^{E397K} mice (Fig. 4D).

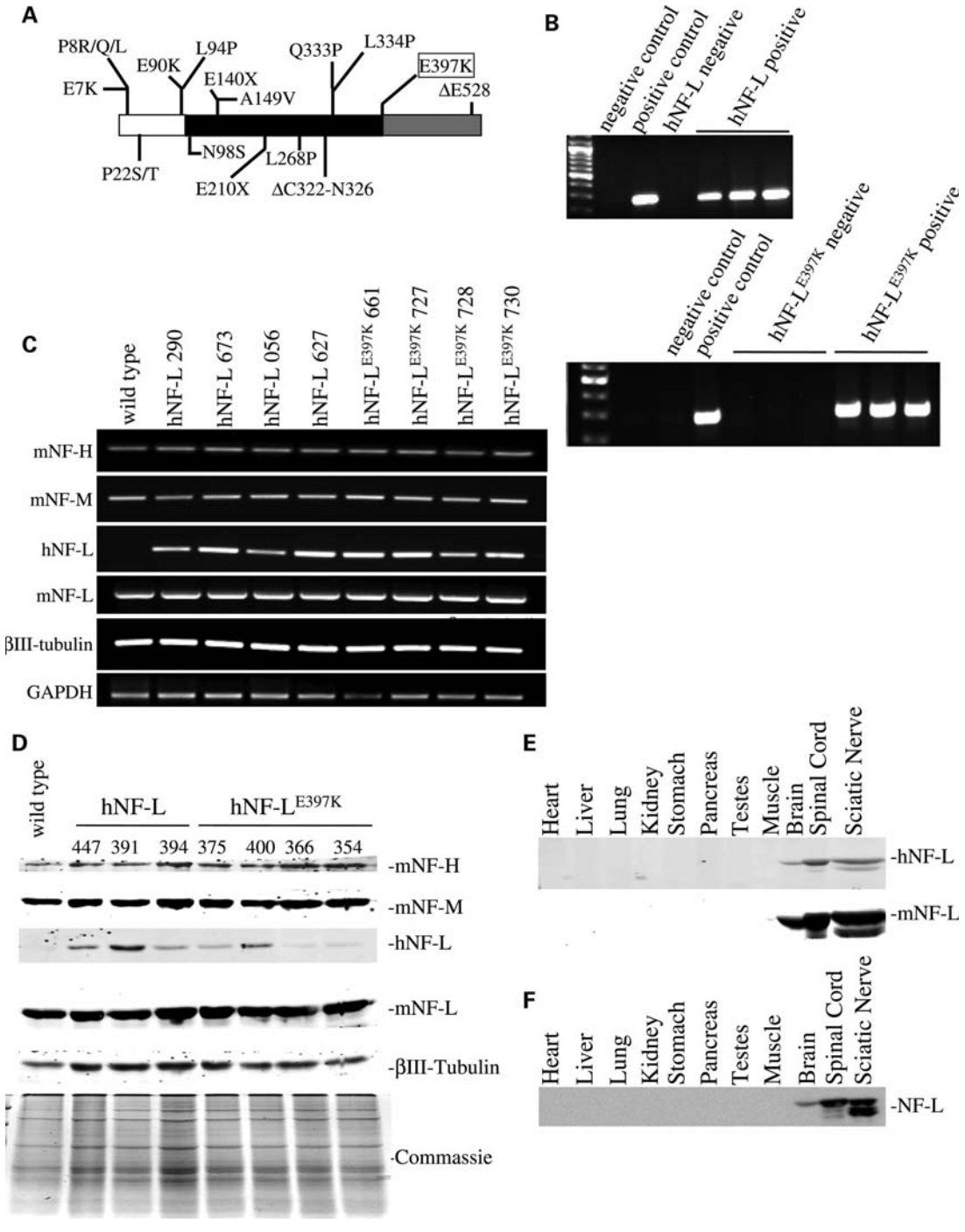

Figure 1. Expression of hNF-L^{E397K} in mice does not affect expression of other cytoskeletal elements. (**A**) Schematic of hNF-L protein with 18 reported mutations indicated. White indicates the N-terminal head domain, black indicates the coil-coiled rod domain and gray indicates the C-terminal tail domain. hNF-L^{E397K} occurs at the end of the rod domain in the most conserved sequence in the intermediate filament family (KLLEGEE). (**B**) Transgenic lines were identified by PCR analysis of genomic DNA derived from tail biopsies. Four lines of hNF-L and hNF-L^{E397K} mice were identified, three of which are shown here. hNF-L was not amplified from wild-type genomic DNA. The endogenous hNF-L promoter drove expression of wild-type and hNF-L. For both upper and lower panels: negative control was no genomic DNA; hNF-L and hNF-L^{E397K} negative controls were wild-type C57Bl6 mice. (**C** and **D**) To determine the effect of expressing wild-type and mutant hNF-L on endogenous mouse cytoskeletal proteins, mRNA (C) and protein (D) levels were analyzed. (C) Expression of hNF-L, hNF-L^{E397K}, mNF-L, NF-M, NF-H and βIII-tubulin was analyzed by reverse-transcription PCR amplification of mRNA purified from spinal cords of wild-type, hNF-L and hNF-L^{E397K} mice. hNF-L transgenes did not alter transcription of other cytoskeletal components. (D) Sciatic nerve lysates were fractionated on 7.5% SDS–polyacrylamide gels from 6-month-old animals and immunoblotted with antibodies recognizing hNF-L (α-NF70kDa), mNF-L (DA2), NF-M (RMO44), NF-H (CPCA-NF-H) and neuron-specific βIII-tubulin (TUJI). Low levels of hNF-L and hNF-L^{E397K} proteins were detected in transgenic mice. hNF-L transgenes did not affect expression of endogenous NF subunits or βIII-tubulin. (**E** and **F**) Utilizing the endogenous hNF-L promoter did not result in ectopic expression of hNF-L transgenes. Lysates from various tissues were fractionated on 7.5% SDS–polyacrylamide gels from 3–4 (E) and 14 (F) months old animals and immunoblotted with an antibody that recognizes both mouse and hNF-L (DA2). All analysis was performed on at least three hNF-L and hNF-L^{E397K} mice.

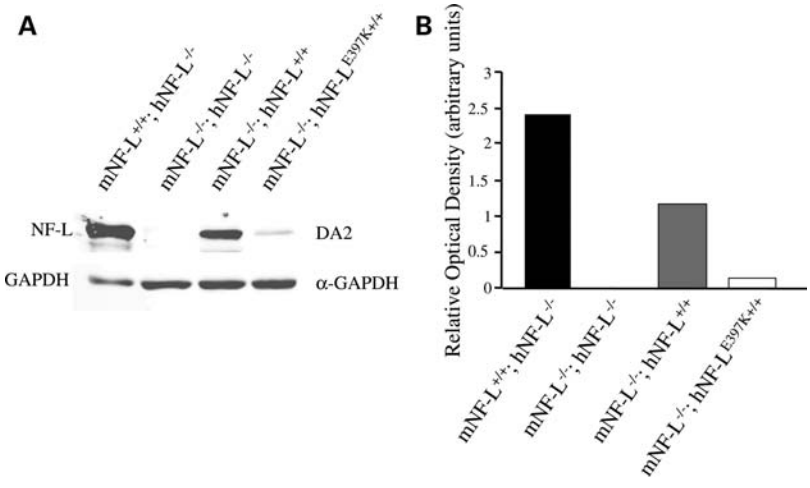

Figure 2. Removal of endogenous NF-L confirms expression of hNF-L and hNF-L^{E397K} transgenes. hNF-L and hNF-L^{E397K} transgenic mice were bred with mNF-L$^{-/-}$ mice to generate mice in which endogenous mouse NF-L is absent in the presence of the hNF-L or hNF-L^{E397K} transgenes. (**A**) Spinal cord lysates were fractionated on 7.5% SDS–polyacrylamide gels from 5–6-month-old animals and immunoblotted with antibodies recognizing mouse and hNF-L (DA2) and GAPDH (α-GAPDH). (**B**) Relative optical densities of NF-L protein normalized to GAPDH levels.

Ectopic phosphorylation of NFs in motor neuron cell bodies occurs early in disease.

Phenotypic analyses were used to validate hNF-L^{E397K} as a model of CMT2E. We then proceeded to conduct a proximal-to-distal analysis of hNF-L^{E397K} nerves to establish cellular alterations that correlate with altered behavior. Ectopic accumulations of NFs are a hallmark of neurodegenerative diseases (24,25). However, for diseases such as amyotrophic lateral sclerosis (ALS), NFs are at most risk factors for disease (26). To determine whether mutations in NF-L lead to ectopic accumulation of phosphorylated NFs, NF accumulation was analyzed over a time course initiated prior to the onset of overt hind limb weakness. Motor neurons were identified with an NF-L-specific antibody (Fig. 5A1–D1), and ectopically phosphorylated NFs were identified with an antibody that recognizes NFs in a phospho-dependent manner (SMI-31, Fig. 5B2–D2). Merged images confirm that ectopic NFs are accumulating in NF-L-positive cells within the ventral horn (A3–D3). NF accumulations were observed in 1 (Fig. 5B1–B3) and 3 (Fig. 5D1–D3) month old hNF-L^{E397K} mice. These accumulations persisted in 6- and 13-month-old hNF-L^{E397K} mice (Supplementary Material, Fig. S1). Increasing the total level of NF-L in mice led to ectopic phosphorylation of NFs (Table 1). However, the number of positive motor neuron cell bodies was increased in hNF-L^{E397K} mice (Table 1). Appearance of ectopically phosphorylated NFs at 1 and 3 months precedes the onset of overt hind limb weakness in hNF-L^{E397K} mice by at least 3 months. Relative to diseases such as ALS, the accumulations observed in hNF-L^{E397K} mice are mild.

Reduced motor nerve conduction velocities and reduced axonal diameter in hNF-L^{E397K} mice

CMT2E patients with the hNF-L^{E397K} variant have reduced motor nerve conduction velocities (MNCVs) in branches of the sciatic nerve (8). Therefore, we measured MNCVs from the sciatic nerve of age-matched hNF-L control and hNF-L^{E397K} mice (Fig. 6A). As with patients, hNF-L^{E397K} mice show a significant reduction in MNCV ($P < 0.03$).

Axonal diameter influences the rate of NCV (27,28). Therefore, the size of all axons within the fifth lumbar ventral and dorsal roots was determined in both hNF-L controls and hNF-L^{E397K} mice. For ease of comparisons, age-matched hNF-L mice are referred to as ‘presymptomatic’ and ‘symptomatic’. This is not to imply that these mice displayed a phenotype. Nerves from hNF-L and hNF-L^{E397K} mice were analyzed prior to and after the development of overt hind limb weakness. Cross-sectional areas (Supplementary Material, Fig. S2) were measured for all axons, and corresponding diameters were calculated. There was no difference in diameter distributions of large motor axons in age-matched hNF-L and hNF-L^{E397K} mice prior to the onset of hind limb weakness (Fig. 6B). However, the peak diameter for small motor axons was reduced by 0.5 μm in presymptomatic hNF-L^{E397K} mice (Fig. 6B). After onset, there was a decrease in the number of small myelinated axons between 1.5 and 2.5 μm and an increase in the number of large myelinated axons between 11 and 14 μm for both age-matched hNF-L and symptomatic hNF-L^{E397K} mice (Fig. 6C). The peak diameter for small myelinated fibers remains reduced by 0.5 μm in symptomatic hNF-L^{E397K} mice (Fig. 6C). Moreover, the peak diameter for large myelinated axons of symptomatic hNF-L^{E397K} mice was also reduced by 0.5 μm relative to the peak diameter in age-matched hNF-L mice (Fig. 6C). Analysis of the total population of motor axons by the Mann–Whitney *U*-test indicates that there is a statistically significant difference in the distribution of axonal diameters in both presymptomatic and symptomatic hNF-L^{E397K} mice. There was no difference in the total number of axons in hNF-L and hNF-L^{E397K} motor roots before or after the onset of symptoms (Fig. 6D).

Expressing hNF-L^{E397K} had no effect on the peak diameter of sensory axons in age-matched hNF-L and presymptomatic hNF-L^{E397K} mice (Fig. 6F). There was a decrease in the

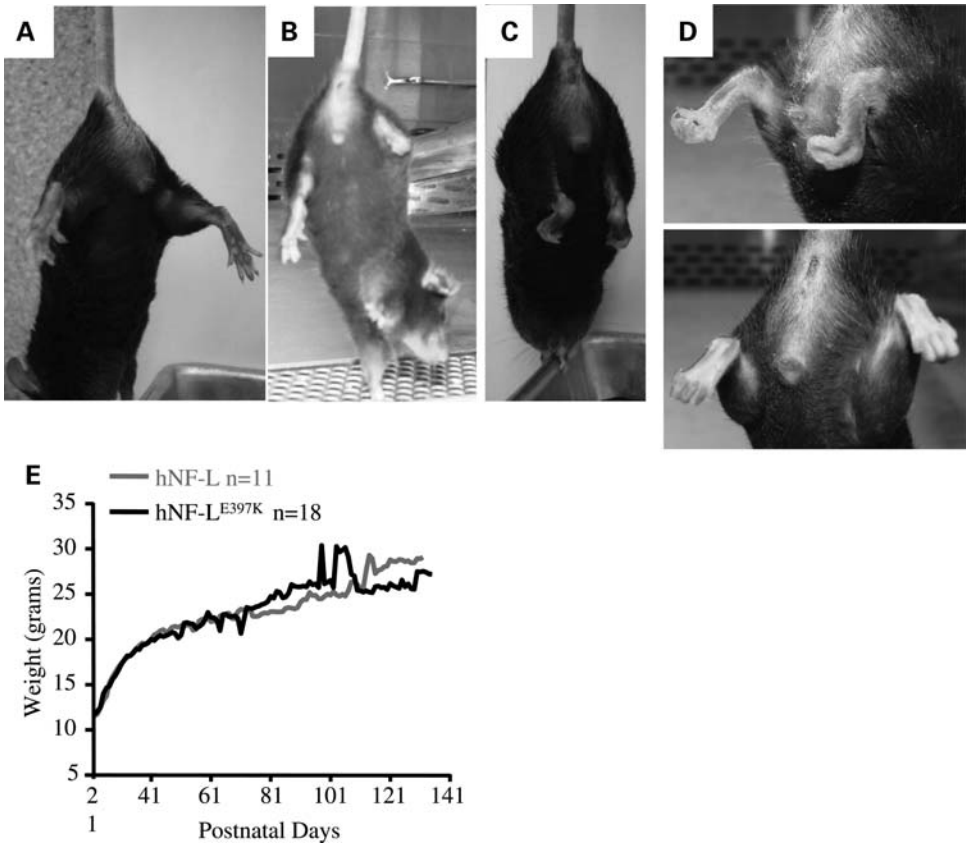

Figure 3. Expression of hNF-L^{E397K} in mice results in aberrant hind limb posture and digit deformities. CMT is associated with aberrant posture of the lower limbs and structural deformities of the feet. To determine whether hNF-L^{E397K} mice developed similar signs of disease, hNF-L and hNF-L^{E397K} mice were induced to spread their hind limbs and digits. (**A**) When lifted by the base of the tail, hNF-L mice spread both hind limbs and digits. (**B**–**C**) However, hNF-L^{E397K} mice were unable to spread their hind limbs. Additionally, the digits on the paws of the hind limbs curled under the paw. This was observed both uni- (B) and bi-laterally (C). (**D**) Close-up of curled digits in hNF-L^{E397K} mice. (**E**) Aberrant hind limb posture and paw deformities were not due to excessive loss of musculature determined by monitoring total weight loss in both hNF-L and hNF-L^{E397K} mice. Weight was monitored by weighing 26 hNF-L and 35 hNF-LE397K mice once per week.

number of axons between 2.5 and 3.0 μm and an increase in the number of axons between 3.5 and 5.0 μm in presymptomatic hNF-L^{E397K} mice (Fig. 6F). After onset, there was no alteration in peak axonal diameter for either age-matched hNF-L or symptomatic hNF-L^{E397K} mice (Fig. 6G). However, the number of axons between 1 and 2.5 μm was decreased in both age-matched hNF-L and symptomatic hNF-L^{E397K} mice relative to younger mice (compare Fig. 6F with G). Additionally, hNF-L^{E397K} mice have decreased number of axons between 4 and 13 μm (Fig. 6G). Analysis of sensory axons distributions by the Mann–Whitney *U*-test indicates that there is statistically significant difference in the distributions of axonal diameters in both presymptomatic and symptomatic hNF-L^{E397K} mice. Symptomatic diameter distributions were further analyzed by two-way ANOVA with Holm–Sidak *post hoc* analysis. This analysis suggests that there is no difference in the number of axons between hNF-L and hNF-L^{E397K} mice at any of the diameters. Therefore, the decrease in large sensory axons observed in symptomatic hNF-L^{E397K} mice is not statistically significant. The total number of sensory axons is not affected prior to the onset of symptoms (Fig. 6H). Symptomatic hNF-L^{E397K} mice have fewer axons than age-matched hNF-L controls (Fig. 6H). However, the difference did not reach statistical significance.

Owing to the relatively mild axonal alterations, the ratio of axon diameter/fiber diameter (*g*-ratio) was measured in 10% of all fifth lumbar motor and sensory axons of symptomatic mice. Axons were randomly selected and localized throughout the entire root. The *g*-ratio in hNF-L^{E397K} motor axons was significantly larger than age-matched hNF-L mice (Fig. 6E). Interestingly, *g*-ratio for hNF-L^{E397K} sensory axons was significantly reduced (Fig. 6I). Although *g*-ratios were significantly altered in hNF-L^{E397K} mice, all measured *g*-ratios were within the optimal range (0.6–0.7) for maximizing neuronal conduction (29). Therefore, this difference is unlikely to explain the observed decrease in MNCV in hNF-L^{E397K} mice.

NFs appear similar in hNF-L and hNF-L^{E397K} motor and sensory axons

NF abnormalities were observed in sural nerve biopsies of hNF-L^{E397K} patients. Some of the axons within the sural nerve had increased NF densities, with the axons appearing swollen

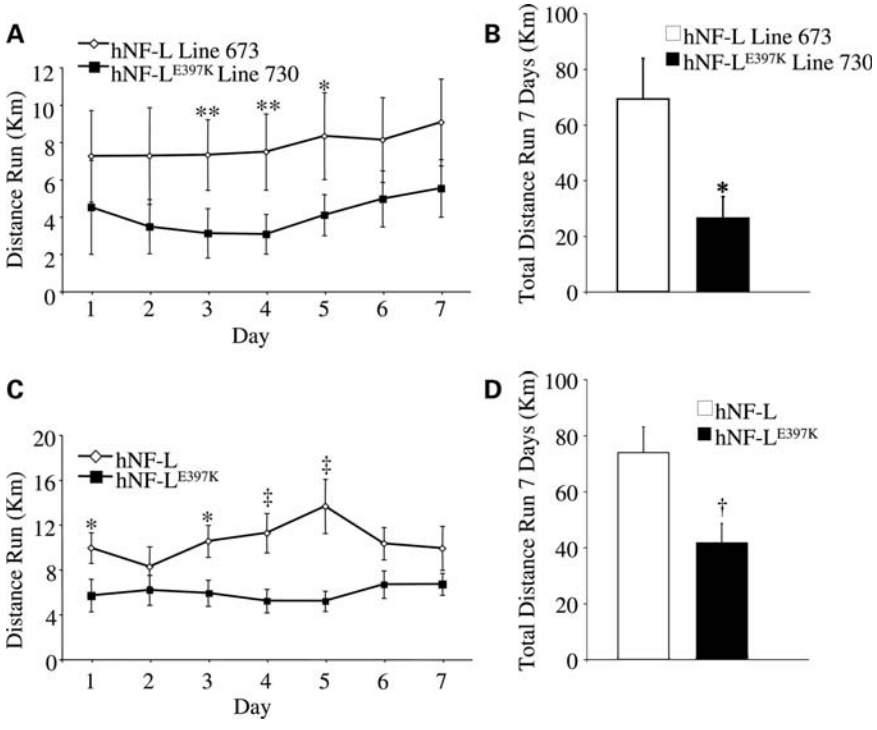

Figure 4. hNF-L^{E397K} mice have reduced voluntary activity. Mice of 1–4 months of age were given free access to running wheels for a period of 7 days. Revolutions were stored on activity wheel counters and then converted into kilometers on the basis of a 5 in. diameter running wheel. (**A**) Daily and (**B**) total activity were monitored in a single line of hNF-L and hNF-L^{E397K} mice. Daily activity was significantly reduced at days 3–5 in line 730 hNF-L^{E397K} relative to line 673 hNF-L. Total activity over 7 days was also significantly reduced. To determine whether reduced activity was unique to line 730, all lines of hNF-L^{E397K} and hNF-L were monitored. (**C**) For all lines of mice, daily activity was significantly reduced relative to control at days 1, 3–5. (**D**) Additionally, total activity over 7 days was significantly reduced in all lines of hNF-L^{E397K} mice. Means for each daily activity were analyzed for overall statistical differences by two-way repeated-measures ANOVA, followed by Holm–Sidak *post hoc* analysis. Means for total distance run were analyzed by unpaired *t*-test. $^{*}P < 0.05$, $^{**}P < 0.02$, $\dagger P < 0.008$, $\ddagger P < 0.005$. For analysis of individual lines, at least six mice were analyzed per genotype. For all lines, at least 13 mice were analyzed for each genotype.

(8). Therefore, we analyzed NFs in both motor and sensory root axons of the fifth lumbar spinal cord of age-matched hNF-L control and symptomatic hNF-L^{E397K} mice (Supplementary Material, Fig. S3). NF organization and number were analyzed in sensory (Fig. 7A and B) as well as small (Fig. 7C and D) and large (Fig. 7E and F) motor axons that were near the peak of the diameter distribution for each class of axons (as shown in Fig. 5). In sensory axons, the peak in NF nearest-neighbor distance (NND) was the same for NFs in hNF-L and hNF-L^{E397K} axons (Fig. 7A). However, within the range of 16–36 nm, hNF-L^{E397K} axons contained fewer NFs, but within the range of 40–64 nm, hNF-L^{E397K} axons contained more NFs. There was no difference in the number of NFs for sensory axons (Fig. 7B).

NF organization was altered in small motor axons (Fig. 7C). The peak in NND was reduced from 32 nm in hNF-L axons to 24 nm in hNF-L^{E397K} axons. Additionally, within the range of 28–34 nm, there are fewer NFs in hNF-L^{E397K} axons. Moreover, small motor axons in hNF-L^{E397K} mice have fewer NFs (Fig. 7D). However, the difference did not reach statistical significance. Within large motor axons, the peak in NND was not altered in hNF-L^{E397K} axons (Fig. 7E). Between 8 and 16 nm, there were fewer NFs, whereas between 28 and 40 nm, there were more NFs in hNF-L^{E397K} axons. As with small motor axons, there were fewer NFs in hNF-L^{E397K} axons (Fig. 7F), but the differences were not statistically significant.

Muscle atrophy without signs of muscle denervation

The hNF-L^{E397K} variant of CMT2E is characterized by atrophy of distal lower limb muscles, which are innervated by branches of the sciatic nerve (8). To determine whether expressing hNF-L^{E397K} in mice resulted in muscle atrophy, muscles of the lower hind limb were isolated, sectioned and stained with hematoxylin and eosin. The gastrocnemius muscle was analyzed prior to (1 month) and after the onset of overt hind limb weakness (4 months). Prior to the onset of hind limb weakness, hNF-L^{E397K} muscle fibers of the gastrocnemius muscle are indistinguishable from wild-type and hNF-L controls (Fig. 8A1–A3). However, by 6 months, hNF-L^{E397K} gastrocnemius muscle fibers are atrophied relative to controls (Fig. 8B1–B3). Muscle fibers of the anterior tibialis (TA) were analyzed in 14-month-old control and hNF-L^{E397K} mice (Fig. 8C1–C3). TA muscle fibers in hNF-L^{E397K} mice are also atrophied (Fig. 8C3). Additionally, hNF-L^{E397K} muscle fibers have increased levels of inclusions within muscle fibers (arrows in Fig. 8C3).

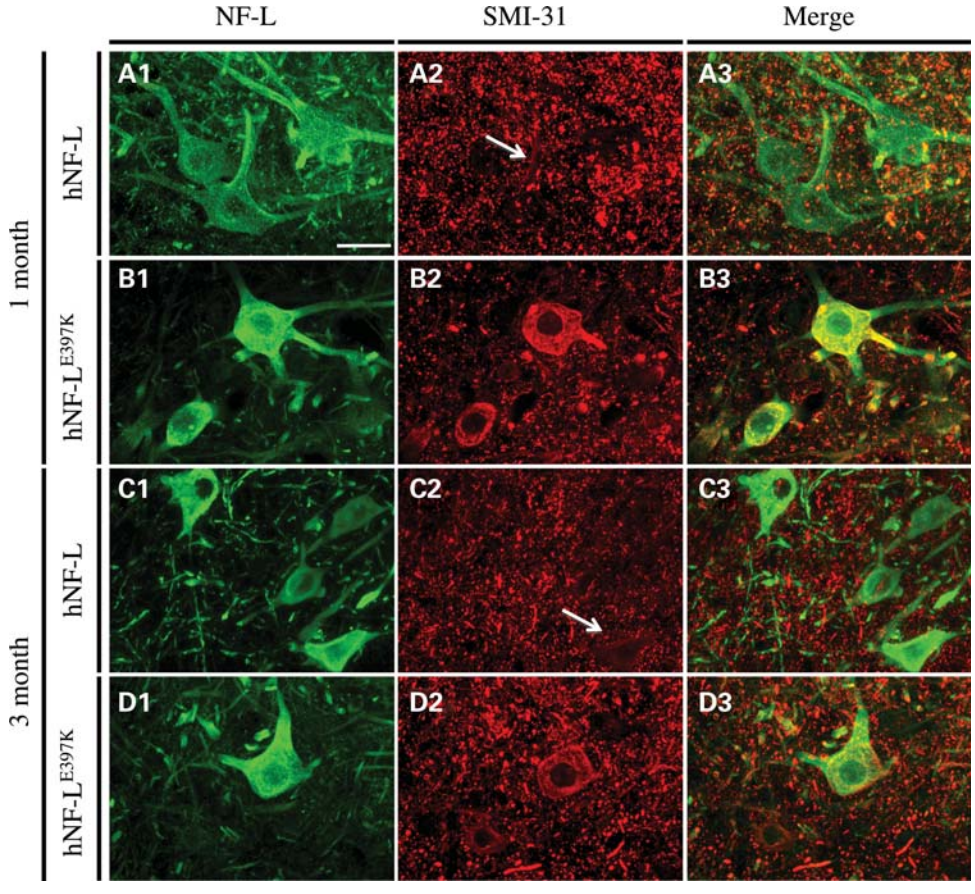

Figure 5. Expressing hNF-L^{E397K} results in ectopic phosphorylation of NFs in motor neuron cell bodies. Lumbar spinal cord sections were immunostained with an antibody to NF-L to identify motor neurons. Ectopically phosphorylated NFs were identified with an antibody that recognizes NFs in a phospho-dependent manner. (**A** and **C**) hNF-L motor neuron cell bodies do not contain ectopically phosphorylated NFs at 1 (A1–A3) and 3 (C1–C3) months of age. (**B** and **D**) However, expression of hNF-L^{E397K} results in ectopic phosphorylation of NFs in motor neuron cell bodies at 1 (B1–B3) and 3 (D1–D3) months. Merged images confirmed that NF accumulations were within NF-L-positive cells (B3 and D3). Scale bar, 50 μm. Spinal cord sections from four to five hNF-L and three hNF-L^{E397K} mice were stained for 1 and 3 month time points.

Muscles of hNF-L^{P22S} mice, the other model for CMT2E, show signs consistent with loss of muscle innervation (22). We analyzed neuromuscular junctions (NMJs) of hNF-L^{E397K} mice to determine whether NFs accumulated at the NMJ, as observed in spinal muscular atrophy (30–32), or whether muscle fibers showed signs of denervation (Fig. 8D and E). NMJs of hNF-L (Fig. 8D) mice were not qualitatively different than NMJs of hNF-L^{E397K} mice (Fig. 8E). None of the NMJs from hNF-L and hNF-L^{E397K} mice had NF accumulations (data not shown). We also counted the number of NMJs that lacked an obvious axon. A total of 100 NMJs were counted for each of four hNF-L mice and four hNF-L^{E397K} mice (Table 2). Although there were NMJs that did not have an associated axon, the number of denervated NMJs was not different between hNF-L and hNF-L^{E397K} mice, suggesting that denervation is not associated with hNF-L^{E397K} pathology (Table 2).

DISCUSSION

NF-L-linked CMT2E mutations span all functional domains of hNF-L (Fig. 1A). A mouse model of CMT2E was recently reported expressing the hNF-L^{P22S} (22) mutation in a highly conserved amino acid located within the N-terminal head domain of NF-L (Fig. 1A). We have now developed and characterized a novel line of mice expressing hNF-L^{E397K}, which is unique as this mutation occurred in the most highly conserved sequence in the intermediate filament family (KLLEGEE), and was located at the end of the rod domain in all intermediate filaments (Fig. 1A).

Utilizing the endogenous hNF-L promoter resulted in low levels of hNF-L that did not affect the expression of endogenous cytoskeletal proteins. Moreover, hNF-L expression was limited to the nervous system in both young and aged mice. As with hNF-L^{P22S} mice (22), hNF-L^{E397K} mice developed signs that were consistent with CMT disease. As early as 4 months, hNF-L^{E397K} mice developed aberrant hind limb posture and digit deformities. Additionally, hNF-L^{E397K} mice had reduced locomotor activity and reduced motor neuron conduction velocity (MNCV). Expressing CMT-linked NF-L mutations did not result in large accumulations of NFs within motor neuron cell bodies [Fig. 5 and reference (22)]. Surprisingly, despite expressing mutations in highly conserved amino acids, the NF network appears largely unaffected [Fig. 7 and reference (22)].

Table 1. Number of motor neuron cell bodies with ectopically phosphorylated NFs

Genotype	SMI-31 positive	Number of motor neurons	Genotype	SMI-31 positive	Number of motor neurons
1 month					
hNF-L	0	25	hNF-L^{E397K}	3	28
hNF-L	1	19	hNF-L^{E397K}	1	29
hNF-L	0	35	hNF-L^{E397K}	4	27
hNF-L	3	42	hNF-L^{E397K}		
Total	4	121	Total	8	84
% Positive	3		% Positive	10	
3 months					
hNF-L	2	45	hNF-L^{E397K}	3	32
hNF-L	1	33	hNF-L^{E397K}	4	37
hNF-L	3	29	hNF-L^{E397K}	16	56
hNF-L	4	31	hNF-L^{E397K}		
Total	10	138	Total	23	125
% Positive	7		% Positive	18	
6 months					
hNF-L	2	21	hNF-L^{E397K}	8	25
hNF-L	0	23	hNF-L^{E397K}	4	22
hNF-L	0	25	hNF-L^{E397K}	6	32
hNF-L	2	30			
hNF-L	4	29			
Total	8	128	Total	18	79
% Positive	6		% Positive	23	
13 months					
hNF-L	0	29	hNF-L^{E397K}	2	25
hNF-L	4	28	hNF-L^{E397K}	2	26
Total	4	57	Total	4	51
% Positive	7		% Positive	8	

In contrast to hNF-L^{P22S} mice, hNF-L^{E397K} muscle fibers of the hind limb displayed indices of muscle pathology such as fiber atrophy. Interestingly, despite the observed alterations in MNCV and muscles, nerves of hNF-L^{E397K} mice were largely unaffected. The peak diameter of small motor axons was reduced prior to the onset of overt hind limb weakness (Fig. 6B). After onset, the peak diameter for both small and large motor axons was reduced by 0.5 μm (Fig. 6C). However, there was no significant loss of motor axons in symptomatic hNF-L^{E397K} mice. Although sensory axons were lost in symptomatic hNF-L^{E397K} mice, the differences did not reach statistical significance. Most of the fiber loss appears to have occurred in large sensory fibers (Fig. 6G). However, none of the observed decreases was statistically significant. Moreover, expressing hNF-L^{E397k} did not result in significant denervation of hind limb muscles, which is also in contrast to hNF-L^{P22S} mice. Therefore, mechanistically it is unclear why hNF-L^{E397K} mice displayed aberrant hind limb posture and muscle pathology. One possibility that cannot be excluded by our current analysis is that aberrant hind limb posture and muscle atrophy could result due to alteration in sensory innervation of muscles. Loss of large sensory axons is also associated with aberrant hind limb posture (33,34).

CMT2E is a heterogeneous disease with onset and severity differing in patients with different NF-L mutations and differing in families with the same mutation (8). Analysis of our mouse model indicated that there were important differences in pathology between hNF-L^{E397K} and hNF-L^{P22S} mice. One of the most striking phenotypic differences was in muscle pathology. hNF-L^{E397K} hind limb muscles were atrophied without significant denervation, whereas hNF-L^{P22S} hind limb muscles were hypertrophic with significant denervation (22). Despite these differences, hNF-L^{E397K} mice developed phenotypes that were consistent with CMT2E patients and hNF-L^{P22S} mice (22), suggesting that pathogenesis of neuropathy in CMT2E may be heterogeneous. The observed differences in cellular pathology between animal models may offer insight into the heterogeneous presentation of CMT2E in patients. These differences may represent a range of possible phenotypes, depending on the severity of a common as yet unidentified pathological trigger.

Our development and characterization of a novel CMT2E animal model revealed similarities in overt phenotypes with important differences in cellular pathology when compared with a previously published mouse model. Given the number of identified NF-L mutations, development and analysis of additional novel lines of CMT2E mice are warranted. Moreover, additional lines may aid in identifying common cellular mechanisms that can be targeted for therapeutic intervention.

MATERIALS AND METHODS

Generation of hNF-L and hNF-L^{E397K} transgenic mice

hNF-L was a generous gift from J.P. Julien. To generate the hNF-L transgenes, we used a ∼9.7 kb genomic fragment of hNF-L, which includes ∼1.7 kb of endogenous 5′ promoter sequence. An *Apa*I/*Hin*dIII fragment was digested out and subcloned into pBlusecript KS [Agilent Technologies (Stratagene), Santa Clara, CA, USA] for site-directed mutagenesis of nucleotide G3332. After confirming mutation of G3332 to A, the *Apa*I/*Hin*dIII fragment was cloned back into the hNF-L genomic fragment to generate the hNF-L^{E397K} DNA fragment. The hNF-L and hNF-L^{E397K} DNA fragments were microinjected into pronuclei of mouse oocytes and implanted into pseudopregnant females. Founders and offspring were genotyped for the hNF-L transgenes by PCR amplification using GoTaq® (Promega, Madison, WI, USA) with the following primers: forward primer—5′-GCACGCAGCTCTTAGGGATA-3′; reverse primer—5′-AGATGATCCGATAGTTGCTG-3′.

Reverse transcriptase PCR amplification of mRNA

Total RNA from spinal cord was extracted with TRIzol reagent according to the manufacturer's protocol (Invitrogen, Carlsbad, CA, USA). RNA extracts were treated with DNAse I (Invitrogen) to prevent genomic contamination of samples and heat-inactivated at 65°C for 5 min. First-strand cDNA synthesis was performed using Superscript III reverse transcriptase (Invitrogen) according to the manufacturer's protocol utilizing 25 ng of total RNA. PCR amplification was performed with GoTaq® (Promega) with the following primer sets: hNF-L: 5′- TACCAAGACCTCCTCAACGTG-3′, 5′-TGGACATCAGATAGGAGCTGG-3′; mNF-L: 5′-CCCTTTCCCTCTTCTCCCCCGTTC-3′, 5′-AAACATCTGTGTGATTCACATTG-3′; mNF-M: 5′-GTCATTTGCGAGAATACCAGG-3′, 5′-tctgacttctcatcttccac-3′; mNF-H: 5′-AGCTGCAAGCCAGGACCACA-3′, 5′-CACTGTCCAGCTGCTGAATAG-3′; βIII-tubulin: 5′-GTGGACTTGG AACCTGGAAC-3′, 5′-CC

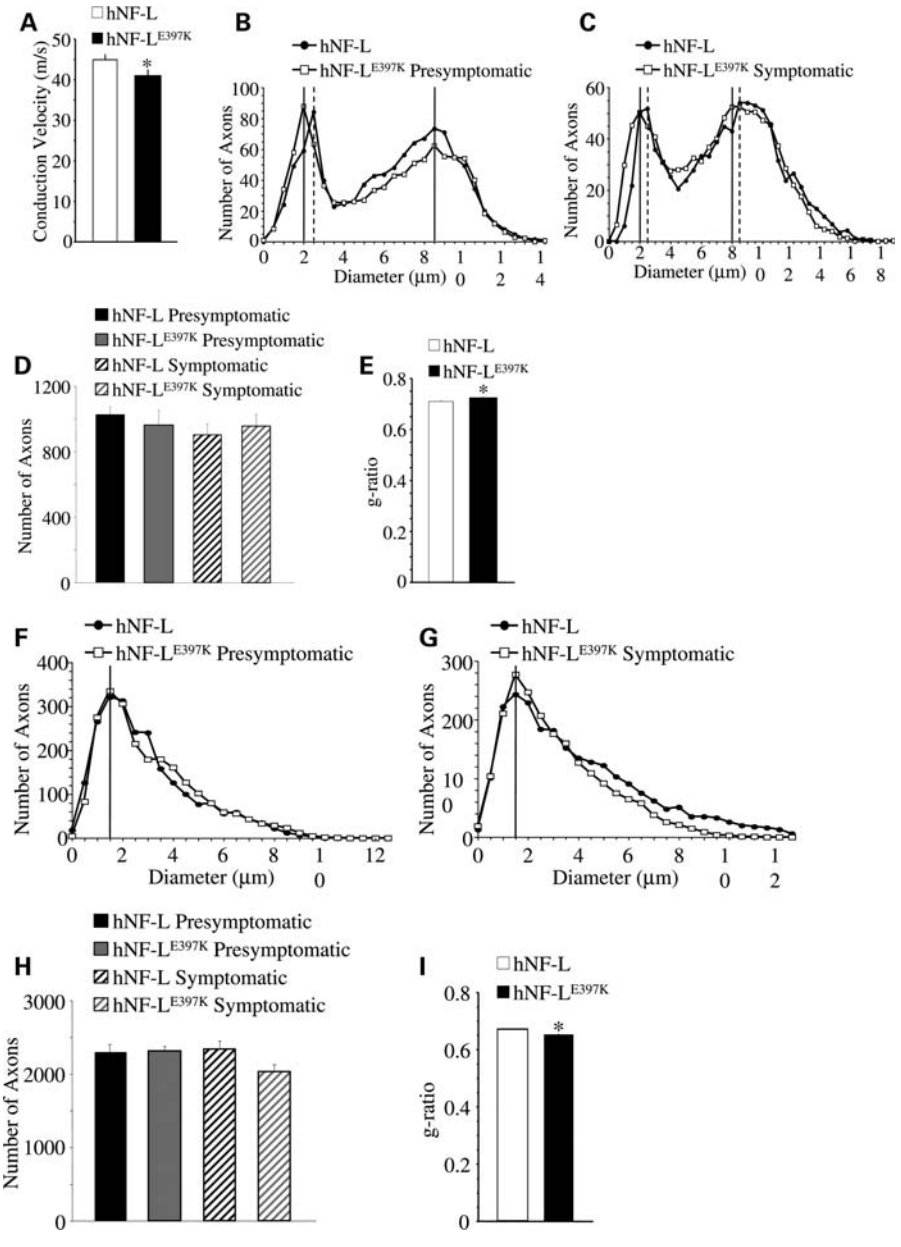

Figure 6. Reduction of MNCV and reduced axonal diameters in hNF-L^{E397K} mice. (**A**) MNCV was measured from axons of the sciatic nerve in hNF-L and hNF-L^{E397K} mice. There was a statistically significant difference between conduction velocities from hNF-L and hNF-L^{E397K} mice. Statistical analysis was performed by unpaired *t*-test. $^{*}P < 0.03$. (**B** and **C**) Distributions of axonal diameters from all axons of the fifth lumbar motor root prior to (B) and after (C) the onset of overt hind limb weakness in age-matched hNF-L and hNF-L^{E397K} mice. The peak diameter for small motor axons was reduced by 0.5 μm prior to the onset of overt hind limb weakness in hNF-L^{E397K} mice (B). After onset, the peak diameter was reduced by 0.5 μm for both small and large motor axons in hNF-L^{E397K} mice (C). Motor axon diameter distributions were analyzed for overall statistical differences utilizing the Mann–Whitney *U*-test. There was a significant difference in diameter distributions between hNF-L and hNF-L^{E397K} mice for both presymptomatic ($P = 0.011$) and symptomatic ($P < 0.001$) time points. (**D**) The total number of axons in the fifth lumbar motor root for age-matched hNF-L and hNF-L^{E397K} mice. Total axon numbers were analyzed for statistical significance by two-way ANOVA. (**E**) The ratio of axon diameter/fiber diameter (*g*-ratio) was analyzed from 10% of all motor axons of symptomatic mice. Axons were randomly selected and localized throughout the entire motor root. *g*-Ratios were analyzed for statistical significance by the Mann–Whitney *U*-test. hNF-L^{E397K} *g*-ratio was significantly larger. (**F** and **G**) Distributions of axonal diameters from all axons of the fifth lumbar sensory root prior to (F) and after (G) the onset of overt hind limb weakness in age-matched hNF-L and hNF-L^{E397K} mice. The peak diameter was unaltered prior to or after the onset of hind limb weakness in sensory axons of hNF-L^{E397K} mice. Sensory axon diameter distributions were analyzed for overall statistical differences utilizing the Mann–Whitney *U*-test. There was a significant difference in diameter distributions between hNF-L and hNF-L^{E397K} mice for both presymptomatic ($P < 0.001$) and symptomatic ($P < 0.001$) time points. (**H**) The total number of axons is reduced in symptomatic hNF-L^{E397K} mice relative to age-matched hNF-L mice. However, the difference did not reach statistical significance. Total axon numbers were analyzed for statistical significance by two-way ANOVA. (**I**) *g*-Ratios were analyzed from 10% of all sensory axons of symptomatic mice. Axons were randomly selected and localized throughout the entire motor root. *g*-Ratios were analyzed for statistical significance by the Mann–Whitney *U*-test. hNF-L^{E397K} *g*-ratio was significantly smaller. MNCVs were measured in a minimum of 15 mice per genotype. Each point represents the averaged distribution of axon diameters from the entire roots of at least three mice for each group. *g*-Ratios were measured on at least three mice per genotype. SEM is reported for all *g*-ratios. However, they are too small to be seen in the figure. SEM motor: hNF-L = 0.005; hNF-L^{E397K} = 0.004; SEM sensory: hNF-L and hNF-L^{E397K} = 0.002.

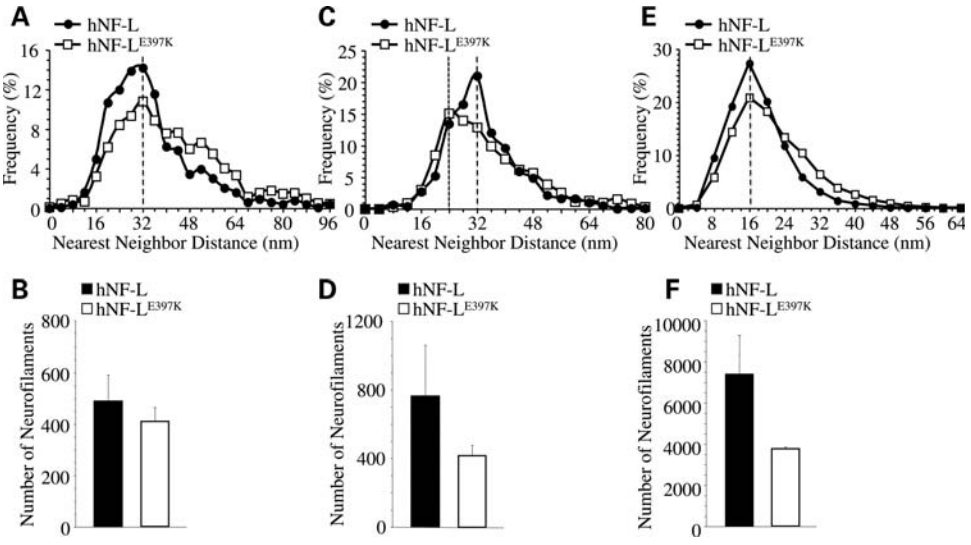

Figure 7. NFs of proximal sensory and small motor axons are altered in mice expressing hNF-L^{E397K}. Axoplasmic organization was analyzed in proximal sensory and motor axons from age-matched hNF-L controls and symptomatic hNF-L^{E397K} mice. Distributions of NND for sensory (**A**) as well as small (**C**) and large (**E**) motor axons from both hNF-L and hNF-L^{E397K} mice. Peak NND was unaffected in both sensory (A) and large motor (E) axons, whereas peak NND in small (C) motor axons was reduced in hNF-L^{E397K} axons. In sensory axons, the number of NFs was reduced between 16 and 36 nm, whereas between 40 and 64 nm NF number was increased in hNF-L^{E397K} axons (A). However, the total number of NFs in sensory nerves was not different between control and hNF-L^{E397K} axons (**B**). For small motor axons, NF number was reduced within the range of 28–34 nm in hNF-L^{E397K} axons (C), and large motor axons had fewer NFs between 8 and 16 nm, whereas they had more NFs between 28 and 40 nm in hNF-L^{E397K} axons (E). Both small (**D**) and large (**F**) motor axons from hNF-L^{E397K} axons had reduced numbers of total NFs. However, these differences were not statistically significant. Total NF numbers were analyzed for statistical significance by Student's *t*-test (sensory axons) and Welch's *t*-test (small and large motor axons). NND was analyzed in at least three mice per genotype in motor axons and four mice per genotype in sensory axons.

TGCAGGCAGTCACAATTC-3′. PCR conditions were as follows: 94°C for 2 min; 35 cycles of 94°C for 30 s, 55°C for 30 s, 72°C for 30 s with 0.5 μM of each primer. Two microliters of reverse transcription reaction solution was added to each PCR reaction, and reverse transcription-PCR-amplified products were electrophoresed on 1.2% agarose gels.

Western blotting

Sciatic nerve and spinal cord tissues were dissected and homogenized on ice in a buffer containing 50 mM Tris, pH 7.5, 0.5 mM EDTA, pH 8, and protease inhibitors were added according to the manufacturer's protocol (Complete Mini, Roche, Mannheim, Germany). An equal volume of a solution containing 50 mM Tris, pH 7.5, 150 mM NaCl, 1% NP-40, 1% sodium deoxycholate and 2% sodium dodecyl sulfate (SDS) was added, and the homogenates were sonicated for 20 s, boiled for 10 min and clarified by centrifugation at 16 000*g* for 10 min. Protein concentration was determined using the Bio-Rad Protein Assay Kit (Bio-Rad, Hercules, CA, USA). Protein extracts were separated on 7.5% SDS–polyacrylamide gels and transferred onto nitrocellulose membrane or stained with Coomassie blue. The hNF-L subunit was identified with a mouse monoclonal antibody specific for human, bovine and porcine NF-L but does not react with rodent NF-L [Anti-NF-70, Chemicon (Millipore), Billerica, MA, USA]. Mouse monoclonal antibodies to NF-L (MCA-DA2, EnCor Biotechnology, Gainesville, FL, USA), NF-M (RMO44, Abcam, Cambridge, MA, USA), GAPDH (monoclonal α-GAPDH Clone GAPDH71.1, Sigma, St Louis, MO, USA) were used to identify each protein. NF-H was identified with a chicken polyclonal antibody that recognizes mammalian subunits (CPCA-NF-H, EnCor Biotechnology). Neuron-specific βIII-tubulin was identified with a rabbit monoclonal antibody (TUJI, Covance, Emeryville, CA, USA). Mouse, chicken and rabbit primary antibodies were detected with donkey anti-mouse, goat anti-chicken and donkey anti-rabbit secondary antibodies conjugated to IR-dye-700×® infrared fluorophores (Rockland, Gilbertsville, PA, USA), respectively. Immunoreactive bands were visualized by infrared detection with an Odyssey image scanner (LI-COR Biosciences, Lincoln, NE, USA).

Activity wheels

Mice of 1–4 months of age were placed in a single activity wheel chamber system (Lafayette Instruments, Lafayette, IN, USA) for 7 days. Activity was measured by the number of revolutions an animal would run during a 24 h period. Revolutions were counted using an optical sensor that detects wheel motion and were stored on an activity wheel counter (Lafayette Instruments). Revolutions were converted into kilometers on the basis of a 5 in. diameter activity wheel. For analysis of individual lines, at least six mice were analyzed per genotype. For all lines, at least 13 mice were analyzed for each genotype. Means for each daily activity were analyzed for overall statistical differences by a repeated-measures ANOVA with Holm–Sidak *post hoc* analysis (SigmaPlot, Systat Software, Inc., San Jose, CA, USA). Means for total distance run were analyzed by unpaired *t*-test (InStat, GraphPad Software, La Jolla, CA, USA). $^{*}P < 0.05$, $^{**}P < 0.02$, $\dagger P < 0.008$, $\ddagger P < 0.005$.

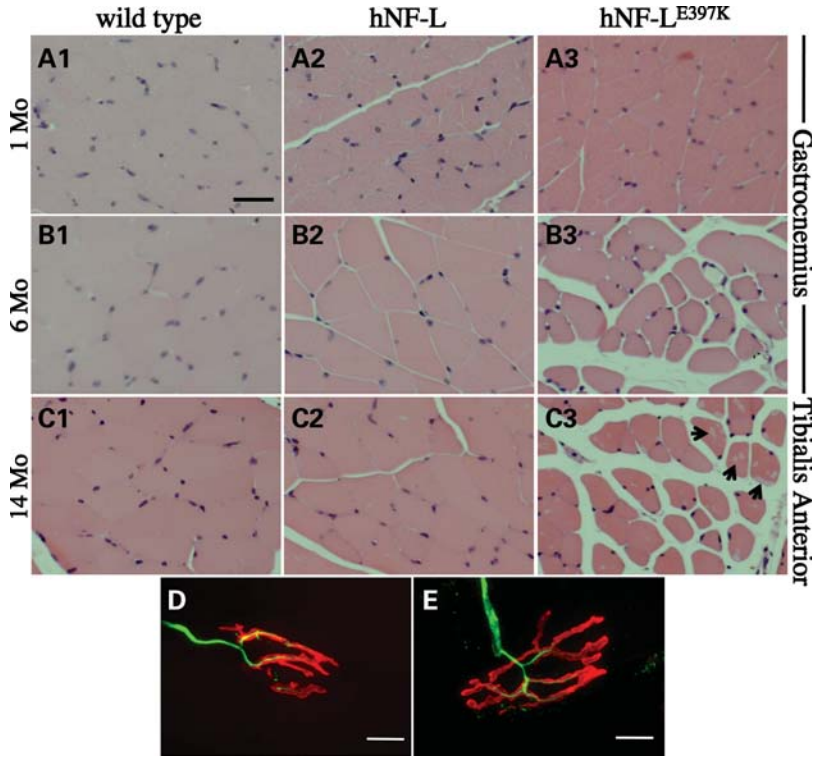

Figure 8. hNF-L^{E397K} mice display progressive muscle atrophy in hind limb muscles without denervation. To determine the morphology of lower hind limb muscles, cross-sections of the gastrocnemius and TA muscles were analyzed from wild-type, hNF-L and hNF-L^{E397K} mice. Muscles were isolated, sectioned and stained with hematoxylin and eosin. (**A**) Gastrocnemius muscle fibers of 1-month-old hNF-L and hNF-L^{E397K} mice were indistinguishable from wild-type mice. Muscle was analyzed at 1 month to determine if muscle pathology was observed prior to the onset of overt phenotypes. (**B**) Gastrocnemius fibers of 6-month-old hNF-L^{E397K} mice were atrophied after the onset of hind limb weakness, whereas hNF-L muscle fibers appeared similar to wild-type mice. (**C**) TA fibers of 14-month-old hNF-L^{E397K} mice were atrophied relative to wild-type and hNF-L mice, suggesting that muscle alterations in the hind limb are not limited to the gastrocnemius. Additionally, the formation of clear inclusions was increased in the muscle of aged hNF-L^{E397K} mice (arrow). Scale bar, 50 μm. (**D** and **E**) Gastrocnemius muscle sections were immunostained with antibodies recognizing NFs (α-NF-L) to identify the axon, and fluorescently conjugated α-bungarotoxin to identify the NMJ. There were no differences in the innervation of NMJs in hNF-L (D) and symptomatic hNF-L^{E397K} (E) mice. Scale bar, 10 μm. Muscle and NMJ analysis was performed on four mice per genotype.

Nerve conduction velocity measurements

Nerve conduction velocities were measured in the sciatic nerve: interosseus muscle system of 12-month-old mice (35). In brief, mice were anesthetized with halothane (4% in O_2 for induction, 2–3% for maintenance), and rectal temperature was maintained at 37°C by a heating lamp and thermal pad connected to a temperature regulator and the rectal thermistor probe. The sciatic nerve was stimulated with single supramaximal square wave pulses (4–8 V and 0.05 ms duration) via fine-needle electrodes placed at the sciatic notch and Achilles tendon. Evoked electromyograms were recorded from the interosseus muscles of the ipsilateral foot via two fine-needle electrodes and displayed on a digital storage oscilloscope. The distance between the two sites of stimulation was measured using calipers, and conduction velocity was calculated as described previously (35). Measurements were made in triplicate from a minimum of 15 animals per genotype, and the median was used as the measure of velocity. Values were compared for overall statistical significance by Student's *t*-test (InStat, GraphPad Software).

Tissue preparation, axon morphological analysis, immunofluorescence and muscle analysis

Mice were perfused intracardially with 4% paraformaldehyde in 0.1 M Sorenson's phosphate buffer, pH 7.2, and post-fixed overnight in the same buffer. Fifth lumbar nerve roots were dissected, treated with 2% osmium tetroxide, washed, dehydrated and embedded in Epon-Araldite resin. Thick sections (0.75 μm) for light microscopy were stained with ρ-phenylenediamine. Cross-sections of fifth lumbar motor and sensory axons were analyzed in at least three mice per group. Axonal diameters were measured using AxioVision Software (Zeiss International). Entire roots were imaged, imaging thresholds were selected individually and the cross-sectional area of each axon was calculated and reported as a diameter of a circle of equivalent area. Axon diameters were grouped into 0.5 μm bins. *g*-Ratios were estimated by measuring the axonal diameter and fiber diameter of individual axons for 10% of all axons per motor and sensory roots, using AxioVision Digital Image Processing Software (Carl Zeiss MicroImaging). Diameter distributions and *g*-ratios were analyzed

Table 2. Number of denervated NMJs

Genotype	Innervate	Denervated	Genotype	Innervate	Denervated
hNF-L	99	1	hNF-L^{E397K}	92	8
hNF-L	97	3	hNF-L^{E397K}	98	2
hNF-L	98	2	hNF-L^{E397K}	98	2
hNF-L	97	3	hNF-L^{E397K}	98	2
Total	391	9	Total	386	14
% Denervated	2		% Denervated	4	

for overall statistical differences by the Mann–Whitney *U*-test (SigmaPlot, Systat Software, Inc.). Sensory axon diameter distributions were further analyzed for statistical significance by two-way ANOVA with Holm–Sidak *post hoc* analysis (SigmaPlot, Systat Software, Inc.).

The total number of axons was analyzed for statistical significance by two-way ANOVA (SigmaPlot, Systat Software, Inc.).

For analysis of motor neuron cell bodies, the lumbar spinal cord was removed, post-fixed overnight with 4% paraformaldehyde and washed in 20% sucrose in phosphate buffer overnight for cryoprotection. Frozen tissues were sectioned with a sliding microtome (Leica Microsystems, Wetzlar, Germany) in 20 μm sections and processed for double-immunofluorescence. Floating sections were incubated in blocking buffer [1% bovine serum albumin, 0.2% fat-free milk, 5% goat serum, 0.5% Triton X-100 in Tris buffered saline (TBS), pH 7.4], followed by antibodies that recognize NF-L (Anti-NF-L, Millipore) (1:200) and phosphorylated epitopes of NFs (SMI31, Covance) (1:1000) diluted in blocking buffer at 4°C overnight. Subsequently, sections were washed and incubated with species-specific secondary antibodies that were conjugated with either Alexa Fluor® 488 or 594 (Molecular Probes, Invitrogen) (1:500) diluted in blocking buffer. Sections were mounted and analyzed on an Olympus DSU confocal microscope (Olympus, Center Valley, PA, USA).

For analysis of muscle fiber morphology, gastrocnemius muscles were isolated and fixed in formalin. Tissues were paraffin-embedded, sectioned into 25 μm thick sections for hematoxylin and eosin staining and mounted. For NMJ analysis, 25 μm thick muscle sections were incubated in blocking buffer and then stained with Alexa Fluor® 594-conjugated α-bungarotoxin (Molecular Probes, Invitrogen) diluted (1:2000) in blocking buffer. After washing with 0.1% Triton X-100 in TBS, sections were then incubated with antibodies recognizing NF-L (α-NF-L, Millipore) (1:200) diluted in blocking buffer. After washing with 0.1% Triton X-100 in TBS, sections were incubated with chicken anti-rabbit secondary antibody conjugated to Alexa Fluor® 488 (Molecular Probes, Invitrogen) (1:500) diluted in blocking buffer. Muscle sections were washed, mounted in Vectashield with DAPI (Vector Labs, Burlingame, CA, USA) and analyzed on an Olympus DSU confocal microscope (Olympus). Complete co-localization of α-bungarotoxin with phosphorylated NF markers was considered muscular innervation, and α-bungarotoxin staining alone represents a denervated junction. A total of 100 NMJs were analyzed per animal slide, with four animals analyzed per genotype.

Electron microscopy and NF nearest-neighbor analysis

For EM analysis, mice were perfused intracardially with 4% paraformaldehyde and 2.5% glutaraldehyde in 0.1 M Sorenson's phosphate buffer, pH 7.2, and post-fixed overnight in the same buffer. Fifth lumbar nerve roots were dissected, treated with 2% osmium tetroxide, washed, dehydrated and embedded in Epon-Araldite resin. Thin sections (60–90 nm) were cut from prepared fifth lumbar root resin blocks with a Leica Ultracut UCT ultramicrotome, collected on grids, stained with 1% aqueous uranyl acetate for 15 min, followed by lead citrate for 2 min. Images of selected axons were collected at 80 kV with a JEOL-1400 transmission electron microscope at magnifications of ×5000, ×10 000 or ×20 000. Raw NF spacing numbers were acquired using IMOD software (University of Colorado, Boulder, CO, USA), and NF NND data were grouped into 4 nm bins using NCMIR Pointzilla (University of California, San Diego, CA, USA). NF numbers were analyzed for statistical significance using Student's *t*-test (sensory axons) or Welch's *t*-test (small and large motor axons) (InStat, GraphPad Software).

SUPPLEMENTARY MATERIAL

Supplementary Material is available at *HMG* online.

ACKNOWLEDGEMENTS

We thank Dr Natalia Karasseva and the University of Missouri-Columbia Transgenic Animal Core for the generation of transgenic founder mice; Ms Lucie Guernsey and Ms Katie Frizzi for technical support; Ms Cheryl Jensen and the University of Missouri EM Core for assistance with tissue preparation for light and electron microscopic analysis; RADIL for hematoxylin and eosin staining of muscle tissues on a re-charge basis; Mr Brian Reigle for writing the scripts used in automated determination of numbers of axons in assigned groups for axonal diameter profiles and Dr David Schulz and Dr Emmanual Liscum for comments and insights that improved this manuscript; Dr D. Cornelison for assistance in imaging of spinal cord immunofluoresence with the confocal microscope; Dr Tsika with assistance in interpreting muscle pathology.

Conflict of Interest statement. None declared.

FUNDING

This work was supported by grants from the National Institutes of Health (NS060073), Charcot–Marie–Tooth Association (C00014627) and University of Missouri Research Board to M.L.G. and by a grant from the National Institutes of Health (DK057629) to N.A.C. Salary support for M.L.G. was provided by the University of Missouri-Columbia and the C.S. Bond Life Sciences Center. H.S. was supported by Charcot–Marie–Tooth Association (C00014627) to M.L.G. D.M.B. was supported by both the C.S. Bond Life Sciences Fellowship Program and the Graduate Assistance in Areas of National Need Fellowship Program. J.M.D. was supported by ARRA supplement to T32 GM008396.

REFERENCES

1. Skre, H. (1974) Genetic and clinical aspects of Charcot–Marie–Tooth's disease. *Clin. Genet.*, **6**, 98–118.
2. Emery, A.E. (1991) Population frequencies of inherited neuromuscular diseases—a world survey. *Neuromuscul. Disord.*, **1**, 19–29.
3. Mersiyanova, I.V., Perepelov, A.V., Polyakov, A.V., Sitnikov, V.F., Dadali, E.L., Oparin, R.B., Petrin, A.N. and Evgrafov, O.V. (2000) A new variant of Charcot–Marie–Tooth disease type 2 is probably the result of a mutation in the neurofilament-light gene. *Am. J. Hum. Genet.*, **67**, 37–46.
4. De Jonghe, P., Mersivanova, I., Nelis, E., Del Favero, J., Martin, J.J., Van Broeckhoven, C., Evgrafov, O. and Timmerman, V. (2001) Further evidence that neurofilament light chain gene mutations can cause Charcot–Marie–Tooth disease type 2E. *Ann. Neurol.*, **49**, 245–249.
5. Georgiou, D.M., Zidar, J., Korosec, M., Middleton, L.T., Kyriakides, T. and Christodoulou, K. (2002) A novel NF-L mutation Pro22Ser is associated with CMT2 in a large Slovenian family. *Neurogenetics*, **4**, 93–96.
6. Yoshihara, T., Yamamoto, M., Hattori, N., Misu, K., Mori, K., Koike, H. and Sobue, G. (2002) Identification of novel sequence variants in the neurofilament-light gene in a Japanese population: analysis of Charcot–Marie–Tooth disease patients and normal individuals. *J. Peripher. Nerv. Syst.*, **7**, 221–224.
7. Jordanova, A., De Jonghe, P., Boerkoel, C.F., Takashima, H., De Vriendt, E., Ceuterick, C., Martin, J.J., Butler, I.J., Mancias, P., Papasozomenos, S. *et al.* (2003) Mutations in the neurofilament light chain gene (NEFL) cause early onset severe Charcot–Marie–Tooth disease. *Brain*, **126**, 590–597.
8. Zuchner, S., Vorgerd, M., Sindern, E. and Schroder, J.M. (2004) The novel neurofilament light (NEFL) mutation Glu397Lys is associated with a clinically and morphologically heterogeneous type of Charcot–Marie–Tooth neuropathy. *Neuromuscul. Disord.*, **14**, 147–157.
9. Abe, A., Numakura, C., Saito, K., Koide, H., Oka, N., Honma, A., Kishikawa, Y. and Hayasaka, K. (2009) Neurofilament light chain polypeptide gene mutations in Charcot–Marie–Tooth disease: nonsense mutation probably causes a recessive phenotype. *J. Hum. Genet.*, **54**, 94–97.
10. Yum, S.W., Zhang, J., Mo, K., Li, J. and Scherer, S.S. (2009) A novel recessive Nefl mutation causes a severe, early-onset axonal neuropathy. *Ann. Neurol.*, **66**, 759–770.
11. Miltenberger-Miltenyi, G., Janecke, A.R., Wanschitz, J.V., Timmerman, V., Windpassinger, C., Auer-Grumbach, M. and Loscher, W.N. (2007) Clinical and electrophysiological features in Charcot–Marie–Tooth disease with mutations in the NEFL gene. *Arch. Neurol.*, **64**, 966–970.
12. Ching, G.Y. and Liem, R.K. (1993) Assembly of type IV neuronal intermediate filaments in nonneuronal cells in the absence of preexisting cytoplasmic intermediate filaments. *J. Cell Biol.*, **122**, 1323–1335.
13. Lee, M.K., Xu, Z., Wong, P.C. and Cleveland, D.W. (1993) Neurofilaments are obligate heteropolymers *in vivo*. *J. Cell Biol.*, **122**, 1337–1350.
14. Yuan, A., Rao, M.V., Sasaki, T., Chen, Y., Kumar, A., Veeranna, Liem, R.K.H., Eyer, J., Peterson, A.C., Julien, J.-P. *et al.* (2006) {alpha}-Internexin is structurally and functionally associated with the neurofilament triplet proteins in the mature CNS. *J. Neurosci.*, **26**, 10006–10019.
15. Ohara, O., Gahara, Y., Miyake, T., Teraoka, H. and Kitamura, T. (1993) Neurofilament deficiency in quail caused by nonsense mutation in neurofilament-L gene. *J. Cell Biol.*, **121**, 387–395.
16. Zhu, Q., Couillard-Després, S. and Julien, J.P. (1997) Delayed maturation of regenerating myelinated axons in mice lacking neurofilaments. *Exp. Neurol.*, **148**, 299–316.
17. Sakaguchi, T., Okada, M., Kitamura, T. and Kawasaki, K. (1993) Reduced diameter and conduction velocity of myelinated fibers in the sciatic nerve of a neurofilament-deficient mutant quail. *Neurosci. Lett.*, **153**, 65–68.
18. Kriz, J., Zhu, Q., Julien, J.P. and Padjen, A.L. (2000) Electrophysiological properties of axons in mice lacking neurofilament subunit genes: disparity between conduction velocity and axon diameter in absence of NF-H. *Brain Res.*, **885**, 32–44.
19. Brownlees, J., Ackerley, S., Grierson, A.J., Jacobsen, N.J., Shea, K., Anderton, B.H., Leigh, P.N., Shaw, C.E. and Miller, C.C. (2002) Charcot–Marie–Tooth disease neurofilament mutations disrupt neurofilament assembly and axonal transport. *Hum. Mol. Genet.*, **11**, 2837–2844.
20. Perez-Olle, R., Leung, C.L. and Liem, R.K. (2002) Effects of Charcot–Marie–Tooth-linked mutations of the neurofilament light subunit on intermediate filament formation. *J. Cell Sci.*, **115**, 4937–4946.
21. Perez-Olle, R., Jones, S.T. and Liem, R.K. (2004) Phenotypic analysis of neurofilament light gene mutations linked to Charcot–Marie–Tooth disease in cell culture models. *Hum. Mol. Genet.*, **13**, 2207–2220.
22. Dequen, F., Filali, M., Lariviere, R.C., Perrot, R., Hisanaga, S. and Julien, J.P. (2010) Reversal of neuropathy phenotypes in conditional mouse model of Charcot–Marie–Tooth disease type 2E. *Hum. Mol. Genet.*, **19**, 2616–2629.
23. Bagby, G.J., Johnson, J.L., Bennett, B.W. and Shepherd, R.E. (1986) Muscle lipoprotein lipase activity in voluntarily exercising rats. *J. Appl. Physiol.*, **60**, 1623–1627.
24. Hirano, A., Donnenfeld, H., Sasaki, S. and Nakano, I. (1984) Fine structural observations of neurofilamentous changes in amyotrophic lateral sclerosis. *J. Neuropathol. Exp. Neurol.*, **43**, 461–470.
25. Hirano, A., Nakano, I., Kurland, L.T., Mulder, D.W., Holley, P.W. and Saccomanno, G. (1984) Fine structural study of neurofibrillary changes in a family with amyotrophic lateral sclerosis. *J. Neuropathol. Exp. Neurol.*, **43**, 471–480.
26. Garcia, M.L., Singleton, A.B., Hernandez, D., Ward, C.M., Evey, C., Sapp, P.A., Hardy, J., Brown, R.H. Jr and Cleveland, D.W. (2006) Mutations in neurofilament genes are not a significant primary cause of non-SOD1-mediated amyotrophic lateral sclerosis. *Neurobiol. Dis.*, **21**, 102–109.
27. Garcia, M.L., Lobsiger, C.S., Shah, S.B., Deerinck, T.J., Crum, J., Young, D., Ward, C.M., Crawford, T.O., Gotow, T., Uchiyama, Y. *et al.* (2003) NF-M is an essential target for the myelin-directed 'outside-in' signaling cascade that mediates radial axonal growth. *J. Cell Biol.*, **163**, 1011–1020.
28. Garcia, M.L., Rao, M.V., Fujimoto, J., Garcia, V.B., Shah, S.B., Crum, J., Gotow, T., Uchiyama, Y., Ellisman, M., Calcutt, N.A. *et al.* (2009) Phosphorylation of highly conserved neurofilament medium KSP repeats is not required for myelin-dependent radial axonal growth. *J. Neurosci.*, **29**, 1277–1284.
29. Waxman, S.G. (1980) Determinants of conduction velocity in myelinated nerve fibers. *Muscle Nerve*, **3**, 141–150.
30. Kong, L., Wang, X., Choe, D.W., Polley, M., Burnett, B.G., Bosch-Marce, M., Griffin, J.W., Rich, M.M. and Sumner, C.J. (2009) Impaired synaptic vesicle release and immaturity of neuromuscular junctions in spinal muscular atrophy mice. *J. Neurosci.*, **29**, 842–851.
31. Kariya, S., Park, G.-H., Maeno-Hikichi, Y., Leykekhman, O., Lutz, C., Arkovitz, M.S., Landmesser, L.T. and Monani, U.R. (2008) Reduced SMN protein impairs maturation of the neuromuscular junctions in mouse models of spinal muscular atrophy. *Hum. Mol. Genet.*, **17**, 2552–2569.
32. Murray, L.M., Comley, L.H., Thomson, D., Parkinson, N., Talbot, K. and Gillingwater, T.H. (2008) Selective vulnerability of motor neurons and dissociation of pre- and post-synaptic pathology at the neuromuscular junction in mouse models of spinal muscular atrophy. *Hum. Mol. Genet.*, **17**, 949–962.

33. Chen, X.J., Levedakou, E.N., Millen, K.J., Wollmann, R.L., Soliven, B. and Popko, B. (2007) Proprioceptive sensory neuropathy in mice with a mutation in the cytoplasmic dynein heavy chain 1 gene. *J. Neurosci.*, **27**, 14515–14524.
34. Dupuis, L., Fergani, A., Braunstein, K.E., Eschbach, J., Holl, N., Rene, F., Gonzalez De Aguilar, J.L., Zoerner, B., Schwalenstocker, B., Ludolph, A.C. *et al.* (2009) Mice with a mutation in the dynein heavy chain 1 gene display sensory neuropathy but lack motor neuron disease. *Exp. Neurol.*, **215**, 146–152.
35. Calcutt, N.A., Tomlinson, D.R. and Biswas, S. (1990) Coexistence of nerve conduction deficit with increased Na(+)-K(+)-ATPase activity in galactose-fed mice. Implications for polyol pathway and diabetic neuropathy. *Diabetes*, **39**, 663–666.